J. Appl. Comput. Mech., 12(3) (2026) 1084-1092
DOI: 10.22055/jacm.2025.48445.5236

ISSN: 2383-4536
jacm.scu.ac.ir

Shahid Chamran University of Ahvaz

Journal of Applied and Computational Mechanics

Research Paper

A Computational Analysis of Sac Volume Effects on Hemodynamics and Rupture Risk in Cerebral Saccular Aneurysms

M. Barzegar Gerdroodbary[1,2], X. Wang[3]

[1] Department of Mechanical Engineering, Iranian Research Organization for Science and Technology (IROST), Tehran, Iran, Email: mbarzegarg@yahoo.com

[2] Department of Electromechanical Engineering, C-MAST-Center for Mechanical and Aerospace Science and Technology, Universidade da Beira Interior, Covilha, Portugal, Email: m.barzegargerdroodbary@ubi.pt

[3] Medical Research Institute/Frontier Science Center for Immunology and Metabolism, Wuhan University, 430072, China, Email: xwang1@proton.me

Received May 10 2025; Revised December 17 2025; Accepted for publication December 17 2025.
✉ Corresponding authors: M. Barzegar Gerdroodbary (m.barzegargerdroodbary@ubi.pt), X. Wang (xwang1@proton.me)

Abstract. This study investigates the influence of aneurysm sac volume on hemodynamic factors associated with rupture risk in patient-specific anterior communicating artery (ACA) aneurysms. Six real patient-specific geometries obtained from the Aneurisk database were analyzed, encompassing a wide range of sac volumes (43–1265 mm^3) while maintaining similar parent vessel radii. Blood flow was modeled using transient Navier–Stokes equations with a one-way fluid–structure interaction (FSI) approach, and the Casson non-Newtonian model was employed to represent viscosity variations associated with hematocrit levels. Three cardiac cycles were simulated under physiologically realistic boundary conditions to ensure temporal convergence. Hemodynamic indices including wall shear stress (WSS), oscillatory shear index (OSI), and sac-averaged velocity, and were evaluated across four characteristic cardiac instants. The results indicate that larger aneurysms exhibit higher sac-averaged velocities but lower localized WSS, with peak WSS concentrated at the ostium in smaller aneurysms and at the dome in larger ones. OSI values were highest near curvature-driven recirculation regions, with overall OSI decreasing as sac volume increased, except in complex multi-dome geometries. Variations in hematocrit demonstrated consistent trends of increasing viscosity leading to higher WSS and pressure but reduced intra-saccular velocity. The findings highlight the critical role of sac volume and geometric complexity in modulating intra-aneurysmal flow structures. Larger volumes tend to distribute hemodynamic stresses more uniformly, whereas smaller sacs display localized high WSS that may predispose them to rupture. These results underscore the need for patient-specific modeling to capture morphological and rheological effects that influence aneurysm stability.

Keywords: ACA aneurysms; Computational modelling; Pulsatile flow; Blood hemodynamic.

1. Introduction

Intracranial saccular aneurysms represent a major cerebrovascular disorder with significant morbidity and mortality, particularly when rupture leads to subarachnoid hemorrhage [1-3]. The mechanisms governing aneurysm initiation, growth, and rupture remain complex, involving an interplay of vascular morphology, hemodynamic forces, and biological remodeling [4, 5]. Among the hemodynamic parameters, wall shear stress (WSS), oscillatory shear index (OSI), and intra-aneurysmal velocity structures have been repeatedly identified as critical indicators of aneurysm stability. Because direct in vivo measurement of these parameters is limited, computational fluid dynamics (CFD) has emerged as a powerful tool to provide detailed insight into flow behavior within patient-specific vascular geometries [6, 7].

Aneurysm sac volume, in particular, plays a vital yet incompletely understood role in modulating intra-aneurysmal flow patterns [8-10]. While previous studies have investigated correlations between aneurysm size and rupture risk, fewer have systematically examined how a broad spectrum of sac volumes affects WSS distribution, OSI behavior, and flow recirculation zones under physiologically realistic conditions. Moreover, complex rheological properties of blood—especially its non-Newtonian behavior at low shear rates—further complicate hemodynamic predictions and warrant careful modeling, such as through the Casson viscosity formulation [11, 12]. These considerations highlight the need for a detailed investigation that simultaneously accounts for geometry, blood rheology, and physiologic pulsatility [13-15]. Figure 1 illustrates the schematic of the blood flow complexity in the saccular region of cerebral aneurysm.

To address these challenges, the present study conducts transient CFD simulations of six patient-specific anterior communicating artery (ACA) aneurysms obtained from the Aneurisk dataset [16]. The cases span a nearly 30-fold range in sac volume while maintaining comparable parent vessel radii, enabling a focused evaluation of how sac size and geometry affect hemodynamic indicators associated with rupture risk. The simulations incorporate pulsatile inlet flow, physiologic hematocrit conditions, and a non-Newtonian Casson model to provide accurate assessment of flow behavior across multiple stages of the cardiac cycle [17-19]. A rigorous mesh-independence study and verification of boundary conditions further ensure the robustness of the numerical predictions [20-22]. The structure of this paper is as follows:

Published online: December 27 2025

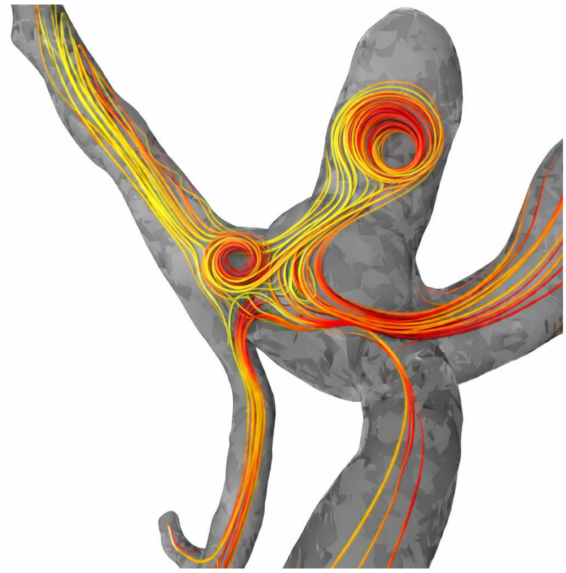

Fig. 1. Schematic of the blood flow streamline in the saccular aneurysm.

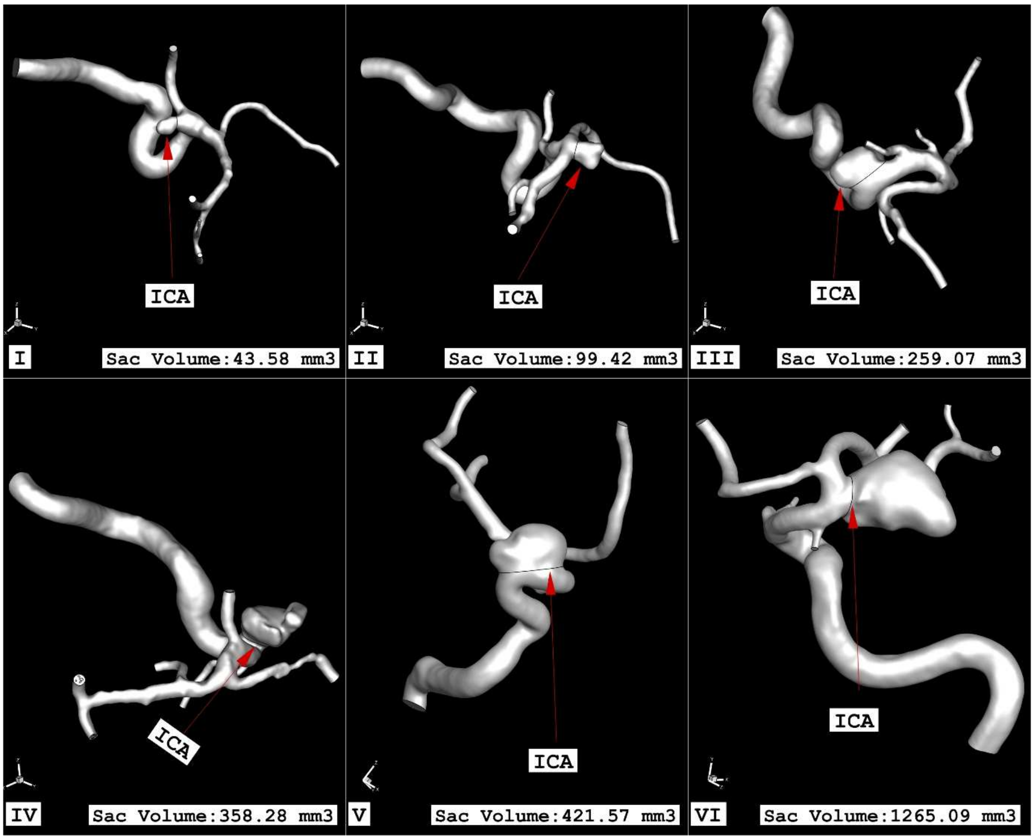

Fig. 2. Geometry definition for all cases.

In Section 2, the selection of aneurysm cases, numerical methodology, rheological modeling, boundary conditions, and grid-independence analysis are described. Section 3 presents the hemodynamic results, including WSS, minimum WSS, OSI, velocity fields, and the effects of hematocrit across the six geometries. Then, section 4 provides a detailed discussion of the observed trends, emphasizing the relationships between sac volume, flow structures, and rupture-associated metrics. Finally, Section 5 concludes the study by summarizing the key findings and outlining opportunities for future research, including improved rheological modeling and validation efforts.

2. Computational Modelling and Simulation

2.1. Aneurysm selections

Figure 2 illustrates the three-dimensional geometries of the selected aneurysms, categorized by sac volume and obtained from the Aneurisk database [16]. The corresponding geometrical characteristics of the saccular ICA aneurysms are summarized in Table 1. Although there is a 10% difference in the parent vessel radius among the cases, it is important to note that the sac volumes we selected span a much broader range, varying from 43 mm³ to 1265.09 mm³—nearly a 30-fold increase.

Table 1. ICA aneurysm geometrical data.

	Case ID	Rupture Status	Age	HCT	Sac Volume (mm^3)
I	62	R	68	0.40	43.58
II	66	UR	58	0.40	99.42
III	14	UR	68	0.40	259.07
IV	64	UR	64	0.40	358.28
V	90	UR	42	0.40	421.57
VI	36	UR	52	0.45	1265.09

This broader variation in sac volume provides a more comprehensive assessment of the hemodynamic behavior under different aneurysmal conditions, which is essential for analyzing intra-aneurysmal flow across various geometries. Since the selected cases are related to the female patients, the applied HCT for the simulation of the cases are 0.4. The age of the patients is within 42 to 68 years old and the first case is related to ruptured aneurysm while other are unruptured ones. In these cases, the mean radius of the parent vessel is near 2 mm.

Although there is a 10% difference in the parent vessel radius among the cases, it is important to note that the sac volumes we selected span a much broader range, varying from 43 mm^3 to 1265.09 mm^3—nearly a 30-fold increase. This broader variation in sac volume provides a more comprehensive assessment of the hemodynamic behavior under different aneurysmal conditions, which is essential for analyzing intra-aneurysmal flow across various geometries. Since the selected cases are related to the female patients, the applied HCT for the simulation of the cases are 0.4. The age of the patients is within 42 to 68 years old and the first case is related to ruptured aneurysm while other are unruptured ones. In these cases, the mean radius of the parent vessel is near 2 mm.

While we acknowledge that the sample size of four patients is limited and not sufficient to draw definitive clinical conclusions, our intent was to focus on identifying trends in hemodynamic behavior across a range of aneurysm sizes. The range of aneurysm sac volumes—from 43 mm^3 to 1265 mm^3—provides a broad spectrum to assess how variations in geometry influence the intra-aneurysmal flow characteristics.

Regarding the inclusion of a ruptured aneurysm, we understand that post-rupture geometric remodeling could impact flow patterns. However, the ruptured case used in our study was obtained from the Aneurisk dataset, which provides the original geometry prior to rupture, as well as information on rupture status. The geometry of the aneurysm in the ruptured case was found to have minimal remodeling or shape changes compared to its unruptured state, based on available clinical records. Thus, the use of this case does not significantly affect the comparability with the other unruptured cases.

2.2. Numerical model

Indeed, 1-way FSI, despite being computationally efficient, has limitations when capturing the full extent of interactions between the fluid and vessel wall, particularly in smaller arterial segments [23-25]. In fact, 2-way FSI is indeed more suitable for regions where fluid flow and wall deformation mutually influence each other, such as smaller vessel segments or aneurysms with highly flexible walls. In our case, the use of 1-way FSI was chosen to maintain computational tractability across multiple cases with varied geometries. This assumption is more appropriate for larger arteries where wall deformation is minimal and has less impact on the flow dynamics [26, 27]. The most common assumption behind the FSI is the constant thickness of the wall of the blood vessel in the entire domain. A thinner wall in the region of smaller vessels produces bigger deformations, leading to higher flow rates [28, 29].

The applied boundary conditions on the inlet and outlet of the blood flow are displayed in Fig. 3. While mass flow rate with demonstrated value are applied on inlet, the pressure with limited changes is applied at outlet of the domain. Four critical stages of the blood flow in the plot of applied mass flow rate are determined. In the peak systolic, the maximum blood flow rate happens. The simulation of the three cardiac cycles are done to ensure the correction of the achieved results and full convergency of the model. The used software for image segmentation was 3D Slicer, reconstruction of the volumetric grids is done by ICEM CFD, and numerical flow solver is ANSYS-FLUENT [30]. The time step for the modeling of the pulsatile blood flow is 2×10^{-4} s.

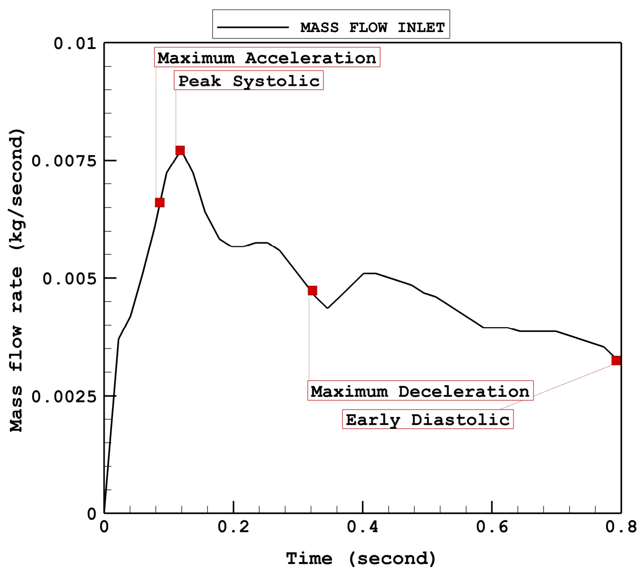

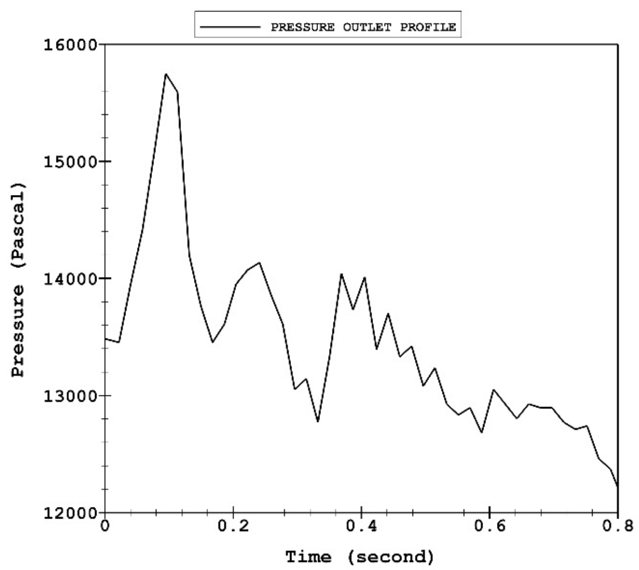

Fig. 3. Applied pressure profile at outlet boundary conditions (One cycle) [31].

Table 2. The results of the wall shear stress.

	Number of cells	Average WSS	Change (%)
Grid 1	1240000	0.2031	-
Grid 2	1880000	0.2122	4.4 %
Grid 3	2424000	0.2191	3.2 %
Grid 4	3910000	0.2211	0.9 %

2.3. Grid independence analysis

In the first step for CFD modeling, high-quality grid for these ICA cases is required. As demonstrated in Fig. 4, the mosaik grid type is used as a type of unstructured grid that is particularly well-suited for the simulation of blood flow inside complex 3D geometries, such as real aneurysms. Mosaik grids are composed of a combination of tetrahedral, prismatic, and hexahedral elements. This hybrid approach allows the grid to better conform to the complex geometry of the aneurysm, improving the accuracy of the simulation. The number of the generated grid for these cases after grid study is between 1.14 million cells and 3.4 million cells. Table 2 presents the mean WSS over aneurysm wall at peak systolic for case I for four different grids. 3rd grid resolution is selected and we applied the same grid size for all other cases. The average non-orthogonality angle was kept below 20°, with a maximum value of 45°, which is within acceptable limits for stable simulations. Non-orthogonal corrections were applied during the discretization process to mitigate any adverse effects on solution accuracy. The average cell skewness was maintained below 0.3, with the maximum value not exceeding 0.5. These values are consistent with best practices for computational fluid dynamics simulations and ensure the robustness of the solution.

The grid independence study has been done using the average of wall shear stress over sac surface. Three different grids are compared with grid sizes of 1140000, 1620000, 2224000 and 3410000 cells. The results of average wall shear stress over sac region are presented in Table 2.

3. Results

The evaluation of the wall shear stress as a critical parameter for the evaluation of the aneurysm risk rupture is done. Since the previous papers [31, 32] have considered minimum WSS as critical index of haemorrhage of the aneurysms, Fig. 5 displays the changes related to the minimum WSS change at diverse stages. The results of min WSS value show that the case 1 and 3 have higher minimum WSS at peak systolic while case 2 has higher WSS on the Maximum acceleration and early diastolic stage.

Figure 6 displays the blood flow structure inside these aneurysms at the defined stages of cardiac cycle. The feature of the blood is shown via iso-velocity surface to enhance the main difference of the blood flow in these models. The formation of the blood structure within the sac region demonstrates the how the blood flow interacts with sac volume and the change of the blood flow in diverse stages of the blood cycle. While the maximum velocity and interaction of the blood is noticed on the peak systolic, the main part of the blood flow happens near the wall since blood flow forms circulation in the aneurysm section [33].

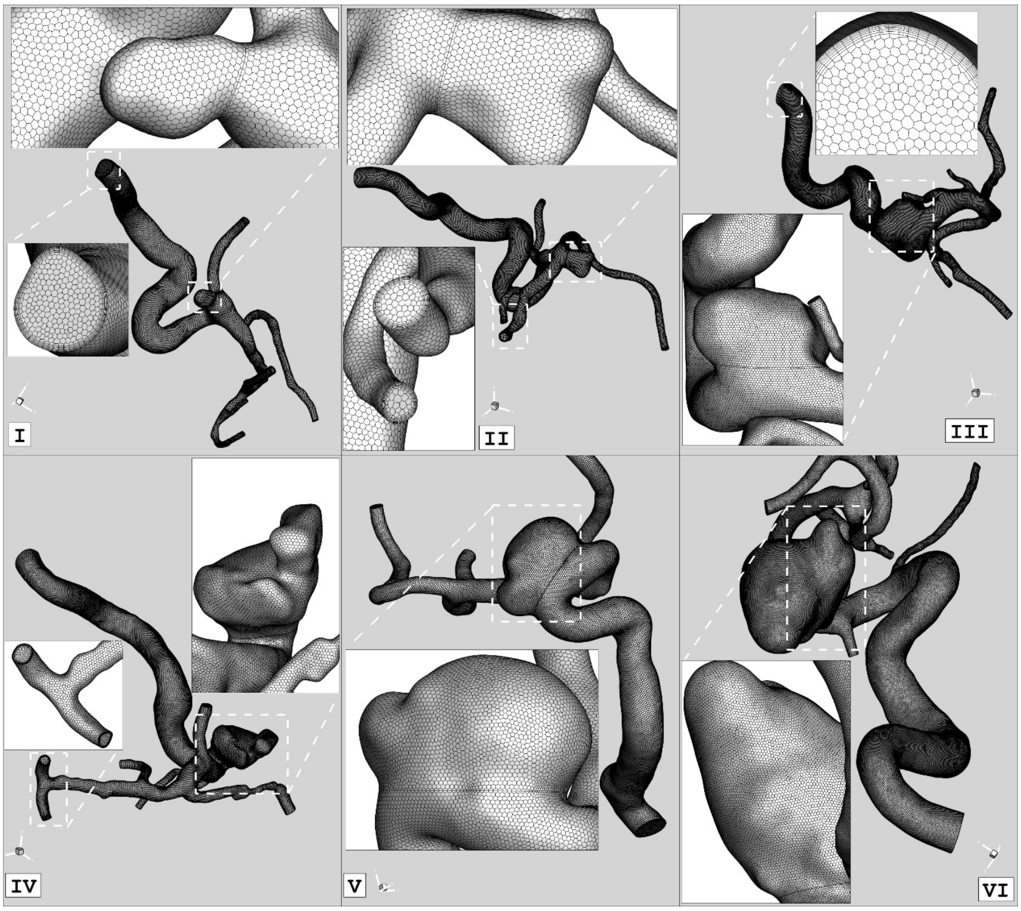

Fig. 4. Grid generation for all cases.

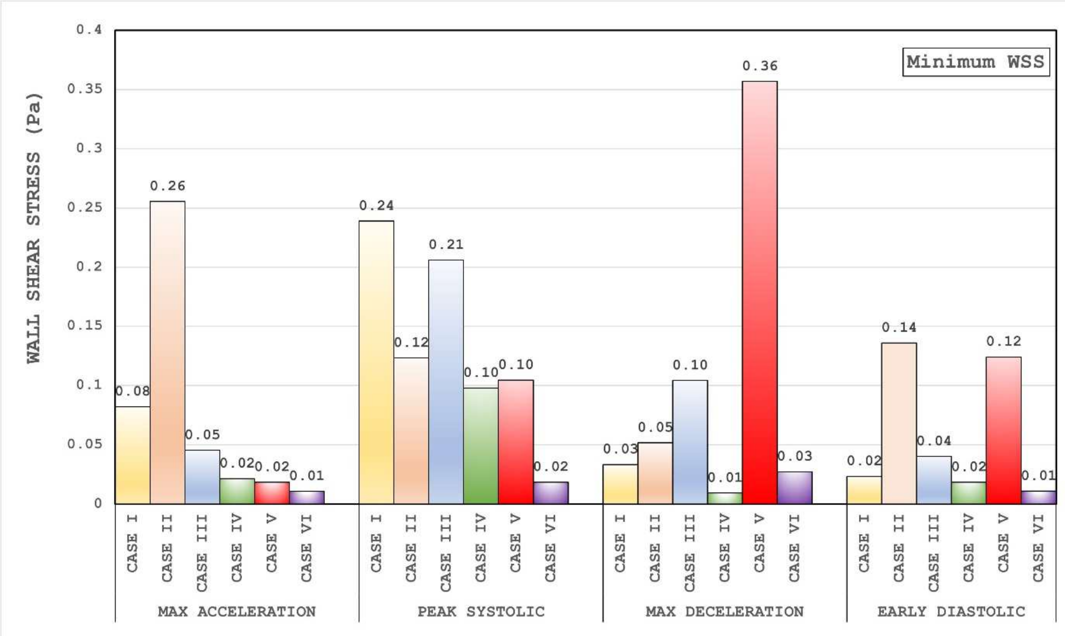

Fig. 5. Variation of Minimum WSS of all cases for four time instants.

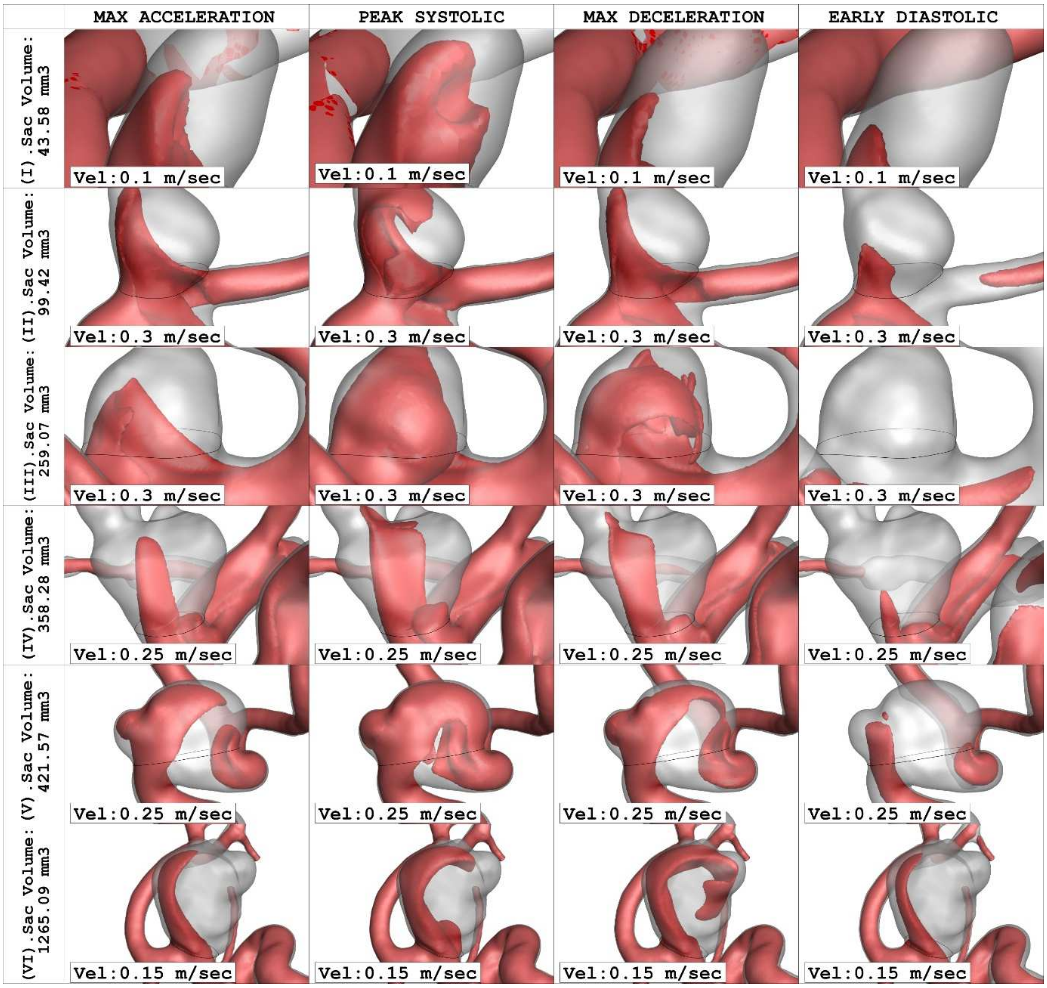

Fig. 6. Velocity ISO-SURFACE of all cases for 4 different time instants.

The comparison of the mean sac velocity at introduced stages are demonstrated in Fig. 7. Comparison of the blood mean velocity inside the sac section indicate that the increasing of the sac volume results in the higher velocity of the blood flow exempt for the case 4. In fact, increasing the sac volume results in the higher inlet area which would increase the velocity of the blood in the sac region. In case 4, the double dome condition would result in lower mean velocity since the blood velocity is considerably low in the second far dome.

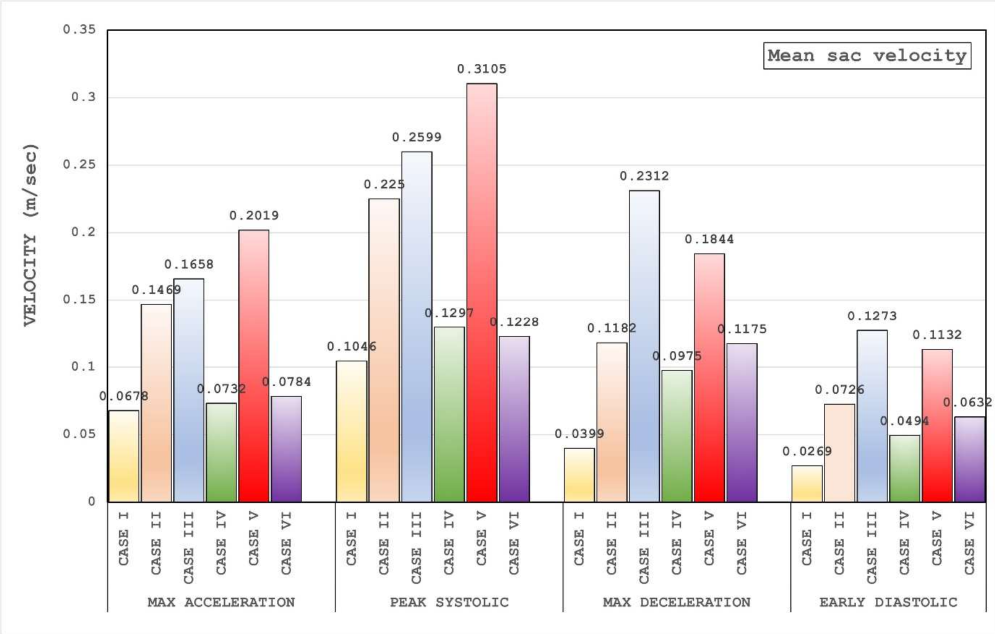

Fig. 7. Mean sac velocity of all cases for 4 different time instants.

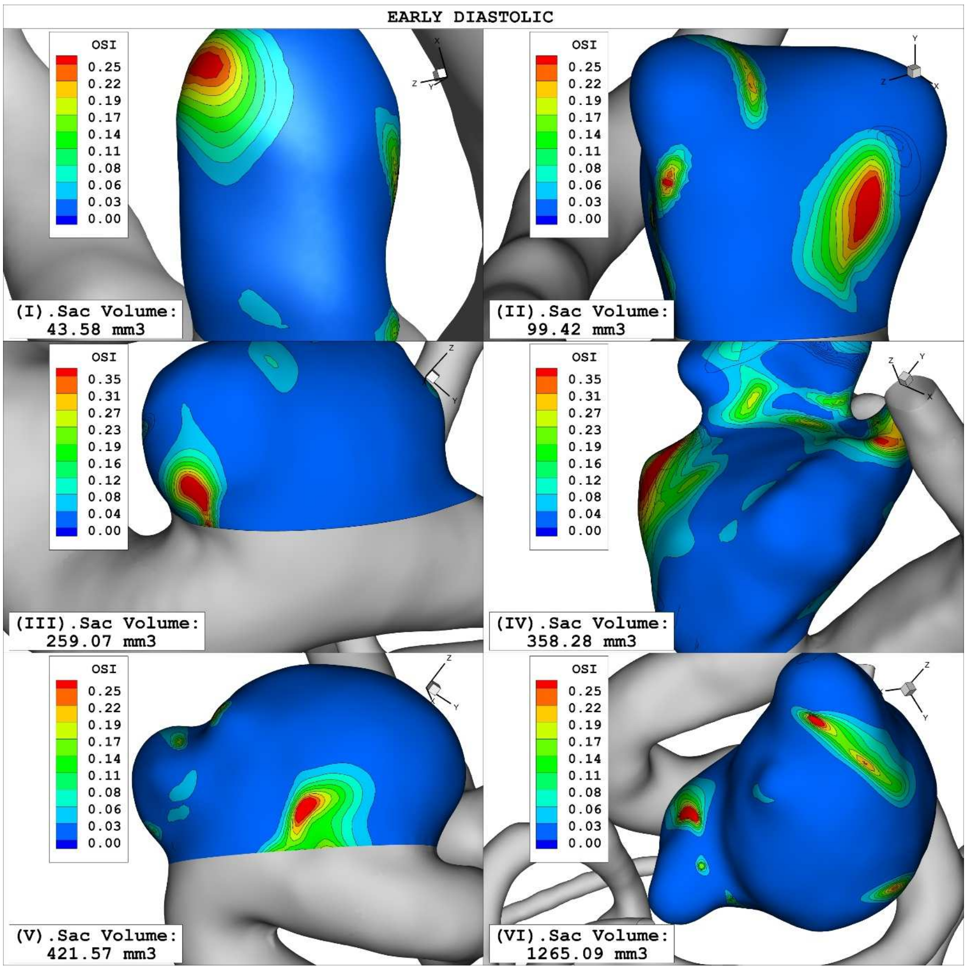

Fig. 8. OSI on aneurysm wall surface of all cases over the entire cardiac cycle.

OSI index is known as critical index for the evaluation of possible aneurysm haemorrhage. This factor is calculated at end of cardiac cycle and Fig. 8 illustrates the distribution of the OSI over the wall for these cases. The value of maximum OSI for the cases are near the region with high curvature. In fact, the region near dome section where the blood flow recirculated is critical from OSI evaluation. In Fig. 8, the value of mean OSI inside the sac region has been compared for these cases. The results of OSI indicate that the OSI value of the case 4 is substantially higher than others. If the last case is exempt from the data due to its double dome configuration, it is found that increasing the sac volume would decrease the OSI over sac surface [34].

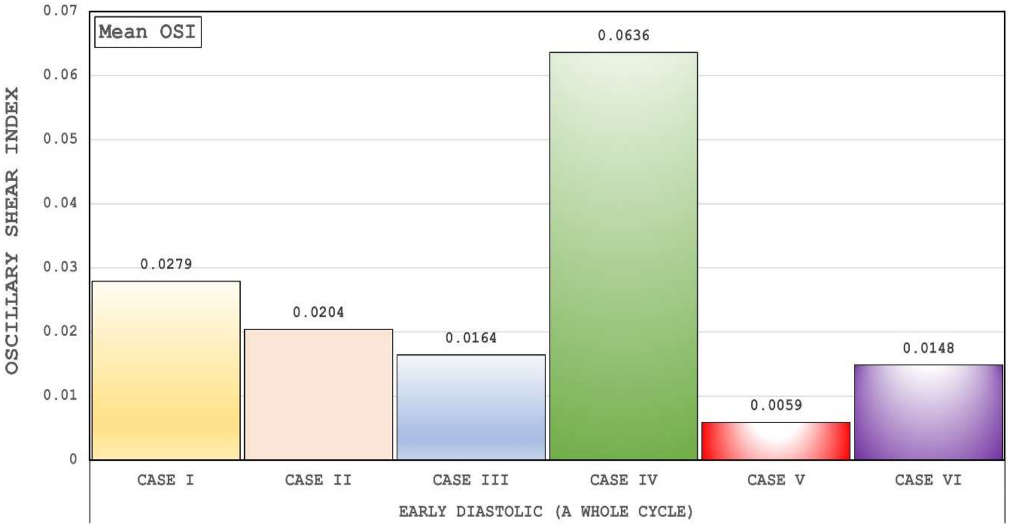

Fig. 9. Mean OSI bar chart of all cases over the entire cardiac cycle.

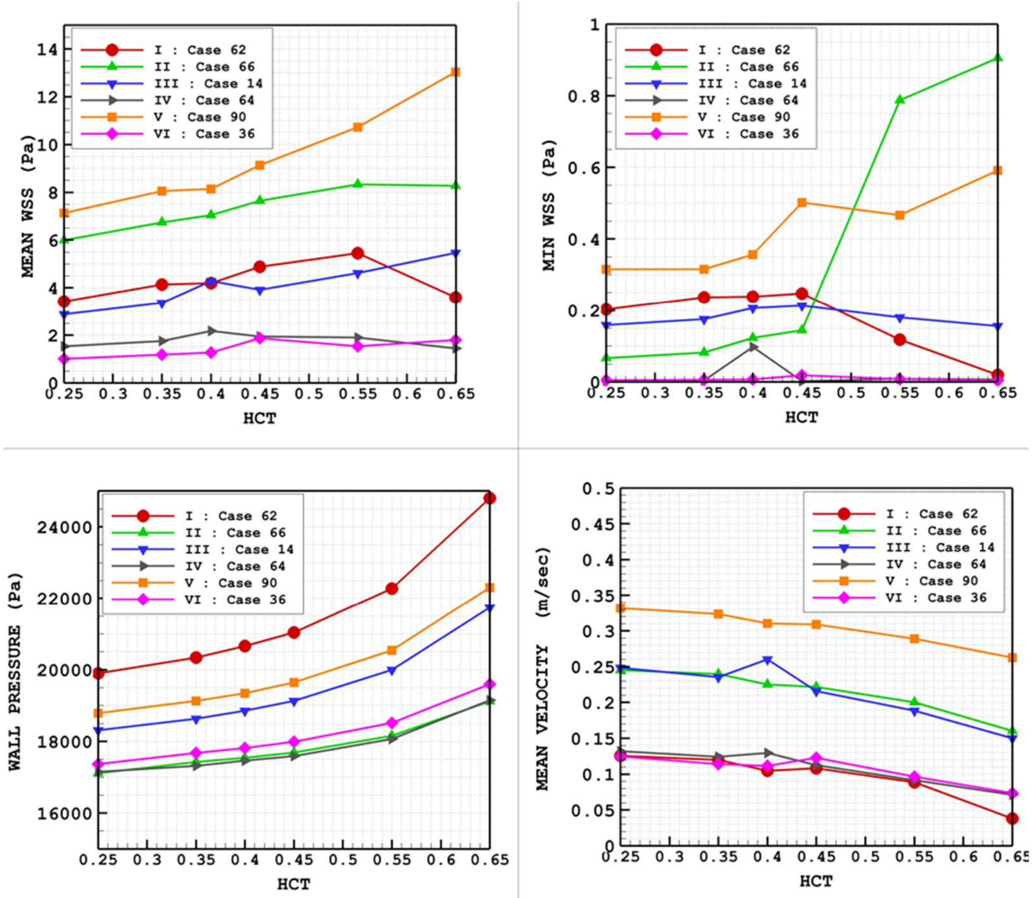

Fig. 10. Effects of blood haematocrit over hemodynamic factors over sac surface of six selected cases.

Figure 10 shows display the effects of hematocrit (HCT) variations on different hemodynamic parameters (mean WSS, minimum WSS, wall pressure, and mean velocity) for six different cases (labeled I to VI). For all cases, mean wall shear stress (WSS) increases as HCT increases. Higher HCT increases blood viscosity, which leads to elevated shear stress at the vessel walls. Minimum WSS shows more variability between cases compared to mean WSS. Low WSS regions are often associated with recirculation zones or areas of slow-moving blood, which are strongly influenced by geometry and local flow dynamics [1]. Wall pressure increases steadily with increasing HCT for all cases. Increased viscosity at higher HCT values enhances resistance to flow, resulting in higher pressures along the vessel walls.

The differences between cases are likely due to variations in aneurysm geometry, which impact flow resistance and pressure distribution. Mean velocity decreases as HCT increases for all cases. Higher viscosity from increased HCT reduces the overall flow velocity as more energy is dissipated to overcome viscous forces. Cases with higher pressure or WSS may be associated with larger or more irregular aneurysms.

4. Discussion

The results provide valuable insights into the hemodynamic behavior and wall shear stress (WSS) patterns in aneurysms with varying sac volumes across different stages of the cardiac cycle. High WSS is concentrated in the ostium region for smaller sac volumes, while larger sac volumes exhibit greater changes in WSS at the dome region, with an overall decrease in WSS as the sac size increases. This trend suggests that high WSS, particularly during peak systolic and maximum acceleration stages, may contribute to endothelial dysfunction and vascular remodeling, potentially driving aneurysm growth and instability. Conversely, the lower WSS observed in larger aneurysms, especially at the dome, might increase the risk of degenerative changes and rupture. The visualization of blood flow structures and streamlines highlights the dynamic interaction between blood flow and aneurysm geometry, with higher sac volumes amplifying blood velocity and circulation patterns within the sac.

The oscillatory shear index (OSI), a critical marker for evaluating aneurysm rupture risk, is predominantly higher near regions of high curvature and recirculation, such as the dome. Although OSI generally decreases with increasing sac volume, exceptional configurations, like the double-dome case, reveal unique hemodynamic behaviors that warrant further investigation. These findings underscore the complex interplay between aneurysm morphology and hemodynamics, emphasizing the importance of patient-specific analyses for assessing rupture risk.

It is important to consider the impact of underlying assumptions on the interpretation of these results. For instance, the rheology of blood, modeled as a Newtonian fluid, may not fully capture the complex, non-Newtonian behavior of blood in regions of low shear rates, which could influence WSS and OSI predictions. Similarly, the location and shape of the aneurysm, which were generalized in this study, may have significant effects on the flow dynamics and associated risks, as demonstrated in previous works. Variations in hematocrit levels, which alter blood viscosity and flow characteristics, are another factor that could impact the accuracy of the predictions. Furthermore, the numerical model employed, including mesh resolution and boundary condition assumptions, may introduce limitations in capturing fine-scale flow structures, particularly in regions of high curvature or complex geometries.

Future work should aim to address these limitations by incorporating non-Newtonian blood rheology models, and variations in hematocrit levels. Additionally, experimental validation of the numerical predictions and more comprehensive studies on the effects of aneurysm morphology and location are essential for improving the reliability of the findings. By refining these aspects and drawing on insights from related studies, the current approach can evolve to provide a more robust framework for assessing aneurysm rupture risks and developing tailored intervention strategies.

5. Conclusion

This study provides a comprehensive hemodynamic assessment of patient-specific ACA aneurysms spanning a wide range of sac volumes. By incorporating realistic geometry, non-Newtonian blood rheology, and pulsatile flow conditions, the results demonstrate that aneurysm sac volume is a dominant morphological factor influencing WSS distribution, OSI behavior, and intra-saccular velocity patterns.

Smaller aneurysms exhibited highly concentrated WSS at the ostium, suggesting localized mechanical fatigue that may contribute to rupture initiation. In contrast, larger aneurysms showed reduced WSS levels but greater hemodynamic complexity within the dome region, where recirculation and low-shear zones can promote degenerative wall changes. The observed decrease in OSI with increasing sac volume—excluding multi-dome configurations—further indicates that geometric complexity can override simple size-based trends. Hematocrit variations also significantly affected viscosity-driven changes in WSS, pressure, and velocity, highlighting the importance of patient-specific blood properties in rupture risk assessment.

Despite the limited sample size, the wide span of sac volumes allowed clear identification of flow behavior trends across different geometric classes. The findings support the use of individualized CFD analyses for clinical evaluation, as generalized metrics may overlook case-specific flow mechanisms. Future work should integrate two-way FSI, advanced non-Newtonian rheology, and experimental validation to improve accuracy and to deepen understanding of aneurysm progression. Overall, this study reinforces that aneurysm rupture risk is governed by a complex interplay of geometry, flow dynamics, and blood rheology, emphasizing the necessity of patient-specific modeling for reliable clinical assessment.

Author Contributions

M. Barzegar Gerdroodbary reviewed the whole manuscript and analyzed the data and revised the manuscript; X. Wang conducted the simulations. The manuscript was written through the contribution of all authors. All authors discussed the results, reviewed, and approved the final version of the manuscript.

Acknowledgments

Not applicable.

Conflict of Interest

The authors declared no potential conflicts of interest concerning the research, authorship, and publication of this article.

Funding

Authors also acknowledge the support by Portuguese national funds by FCT - Foundation for Science and Technology, I.P., within the unit C-MAST - UIDB/00151/2020 (https://doi.org/10.54499/UIDB/00151/2020) and UIDP/00151/2020 (https://doi.org/10.54499/UIDP/00151/2020).

Data Availability Statements

The datasets generated and/or analyzed during the current study are available from the corresponding author on reasonable request.

References

[1] Cebral, J.R., Pergolizzi, R.S., Putman, C.M., Computational fluid dynamics modeling of intracranial aneurysms: qualitative comparison with cerebral angiography, *Academic Radiology*, 14(7), 2007, 804–813.
[2] Shiryanpoor, I., Kheiri, A., Barzegar Gerdroodbary, M., Valipour, P., Moradi, R., Using computational fluid dynamic for evaluation of rupture risk of micro cerebral aneurysms in the growth process: Hemodynamic analysis, *International Journal of Modern Physics C*, 36(2), 2025, 2450184.
[3] Jiang, H., Lu, Z., Barzegar Gerdroodbary, M., Sabernaeemi, A., Salavatidezfouli, S., The influence of sac centreline on saccular aneurysm rupture: computational study, *Scientific Reports*, 13(1), 2023, 11288.
[4] Castro, M.A., Ahumada Olivares, M.C., Putman, C.M., Cebral, J.R., Unsteady wall shear stress analysis from image-based computational fluid dynamic aneurysm models under Newtonian and Casson rheological models, *Medical & Biological Engineering & Computing*, 52, 2014, 827–839.
[5] Lee, U.Y., Chung, G.H., Jung, J., Kwak, H.S., Size-dependent distribution of patient-specific hemodynamic factors in unruptured cerebral aneurysms using computational fluid dynamics, *Diagnostics*, 10(2), 2020, 64.
[6] Khan, P.M., Sharma, S.D., Chakraborty, S., Roy, S., Effects of hematocrit levels on flow structures and stress levels in the healthy and diseased carotid arteries, *Physics of Fluids*, 36(1), 2024, 011907.
[7] Mousavi, S.V., Barzegar Gerdroodbary, M., Sabernaeemi, A., Salavatidezfouli, S., Valipour, P., Impacts of the aneurysm deformation induced by stent on hemodynamic of blood flow in saccular internal carotid artery aneurysms, *AIP Advances*, 14(9), 2024, 095035.
[8] Rostamian, A., Fallah, K., Rostamiyan, Y., Reduction of rupture risk in ICA aneurysms by endovascular techniques of coiling and stent: numerical study, *Scientific Reports*, 13(1), 2023, 7216.
[9] Antoniou, G.A., Alfahad, A., Antoniou, S.A., Torella, F., Prognostic significance of aneurysm sac shrinkage after endovascular aneurysm repair, *Journal of Endovascular Therapy*, 27(5), 2020, 857–868.
[10] Cebral, J.R., Castro, M.A., Burgess, J.E., Pergolizzi, R.S., Sheridan, M.J., Putman, C.M., Characterization of cerebral aneurysms for assessing risk of rupture by using patient-specific computational hemodynamics models, *American Journal of Neuroradiology*, 26(10), 2005, 2550–2559.
[11] Munarriz, P.M., Navarro-Main, B., Alén, J.F., Jiménez-Roldán, L., Castaño-Leon, A.M., Moreno-Gómez, L.M., Paredes, I., et al., The influence of aneurysm morphology on the volume of hemorrhage after rupture, *Journal of Neurosurgery*, 136(4), 2021, 1015–1023.
[12] Jou, L.D., Wong, G., Dispensa, B., Lawton, M.T., Higashida, R.T., Young, W.T., Correlation between lumenal geometry changes and hemodynamics in fusiform intracranial aneurysms, *American Journal of Neuroradiology*, 26, 2005, 2357–2363.
[13] Steinman, D.A., Milner, J.S., Norley, C.J., Lownie, S.P., Holdsworth, D.W., Image-based computational simulation of flow dynamics in a giant intracranial aneurysm, *American Journal of Neuroradiology*, 24, 2003, 559–566.
[14] Barzegar Gerdroodbary, M., Salavatidezfouli, S., Predictive surrogate model of blood hemodynamics for patient-specific carotid artery stenosis, *Journal of the Royal Society Interface*, 22(224), 2025, 20240774.
[15] Barzegar Gerdroodbary, M., Salavatidezfouli, S., A predictive surrogate model based on linear and nonlinear solution manifold reduction in cardiovascular FSI: A comparative study, *Computers in Biology and Medicine*, 189, 2025, 109959.
[16] AneuriskWeb Project, Aneurisk database, Emory University, Department of Mathematics and Computer Science, 2012. Available at: http://ecm2.mathcs.emory.edu/aneuriskweb
[17] Ali, R., Hassan, H.I., Sharma, A., Dhawan, A., Sharma, P., Taher, W.M., Alwan, M., Al-Hussainy, A.F., Mushtaq, H., Heaie, T., Efficiency of endovascular coiling on the evolution of MCA cerebral aneurysm by hemodynamic analysis: Computational study, *International Journal of Modern Physics C*, 37(2), 2026, 2550065.
[18] Sadeh, A., Kazemi, A., Bahramkhoo, M., Barzegar Gerdroodbary, M., Computational analysis of the blood hemodynamic inside internal cerebral aneurysm in the existence of endovascular coiling, *International Journal of Modern Physics C*, 34(05), 2023, 2350059.
[19] Sadeh, A., Kazemi, A., Bahramkhoo, M., et al., Computational study of blood flow inside MCA aneurysm with/without endovascular coiling, *Scientific Reports*, 13, 2023, 4560.
[20] Poueinak, M.M., Abdollahi, S.A., Alizadeh, A., Ahmadpour Youshanlui, M., Zekri, H., Barzegar Gerdroodbary, M., Computational study of blood hemodynamic in ICA aneurysm with coiling embolism, *International Journal of Modern Physics C*, 34(6), 2023, 2350138.
[21] Qin, S., Wu, B., Liu, J., Shiu, W.-S., Yan, Z., Chen, R., Cai, X.-C., Efficient parallel simulation of hemodynamics in patient-specific abdominal aorta with aneurysm, *Computers in Biology and Medicine*, 136, 2021, 104652.
[22] Ding, J., Valipour, P., Impacts of coiling technique on hemodynamic of the MCA aneurysms: Computational study, *International Journal of Modern Physics C*, 35(5), 2024, 2450057.
[23] Valipour, P., Effects of coiling embolism on blood hemodynamics of MCA aneurysms: a numerical study, *Scientific Reports*, 12(1), 2022, 22029.
[24] Rajhi, W., Ahmed, Z., Basem, A., Alizadeh, A., Hussein, S.A., Rajab, H., Louhichi, B., Aich, W., Hemodynamic response to stent-induced aneurysm deformation in patient-specific internal carotid artery cases: A computational study, *Scientific Reports*, 2025, https://doi.org/10.1038/s41598-025-30538-9.
[25] Djuansjah, J., Omar, I., Alizadeh, A., Sadeq, A.M., Hussein, S.A., Singh, N.S.S., Rajab, H., Hajlaoui, K., Dynamic mode decomposition-based surrogate modeling of wall shear stress in aneurysmal arteries, *Physics of Fluids*, 37(8), 2025, 081917.
[26] Cai, Z., Wei, W., Computational analysis of bleb-induced hemodynamic disturbances in cerebral aneurysms, *Chinese Journal of Physics*, 98, 2025, 834–849.
[27] Voss, S., Beuing, O., Janiga, G., Berg, P., Stent-induced vessel deformation after intracranial aneurysm treatment: a hemodynamic pilot study, *Computers in Biology and Medicine*, 111, 2019, 103338.
[28] Karnam, Y., Mut, F., Robertson, A.M., Kaneko, N., Cebral, J.R., Competing pathways of intracranial aneurysm growth: linking regional growth distribution and hemodynamics, *Journal of Neurosurgery*, 142(6), 2025, 1741–1750.
[29] ANSYS Inc., ANSYS® Fluent User's Guide, Release 2020 R2, Canonsburg, PA, 2020.
[30] Malvè, M., Chandra, S., García, A., Mena, A., Martínez, M.A., Finol, E.A., Doblaré, M., Impedance-based outflow boundary conditions for human carotid haemodynamics, *Computer Methods in Biomechanics and Biomedical Engineering*, 17(11), 2014, 1248–1260.
[31] Xu, L., Liang, F., Zhao, B., Wan, J., Liu, H., Influence of aging-induced flow waveform variation on hemodynamics in aneurysms present at the internal carotid artery: A computational model-based study, *Computers in Biology and Medicine*, 101, 2018, 51–60.
[32] Silva, M.L.F., Gonçalves, S.F., Haniel, J., Lucas, T.C., Huebner, R., Comparative study between 1-way and 2-way coupled fluid-structure interaction in numerical simulation of aortic arch aneurysms, *Anais da Academia Brasileira de Ciências*, 95(Suppl. 1), 2023, e20210859.
[33] Kuharat, S., Chaudhry, M.A., Bég, O.A., Bég, T.A., Computational hemodynamic simulation of non-Newtonian fluid-structure interaction in a curved stenotic artery, *European Mechanical Science*, 8(4), 2024, 226-256.

ORCID iD

M. Barzegar Gerdroodbary https://orcid.org/0000-0002-8243-9476
X. Wang https://orcid.org/0009-0009-6429-1278

How to cite this article: Barzegar Gerdroodbary M., Wang X. A Computational Analysis of Sac Volume Effects on Hemodynamics and Rupture Risk in Cerebral Saccular Aneurysms, *J. Appl. Comput. Mech.*, 12(3), 2026, 1084-1092. https://doi.org/10.22055/jacm.2025.48445.5236